Coronal Structure of Star-Like Block Ionomer Micelles: An Investigation by Small-Angle Neutron Scattering

Matthew Moffitt,[†] Yisong Yu,[‡] Diep Nguyen,[§] Vito Graziano,[⊥] Dieter K. Schneider,[⊥] and Adi Eisenberg*[,‡]

Department of Chemistry, McGill University, 801 Sherbrooke St. West, Montreal, P.Q., Canada, H3A 2K6, and Departments of Physics and Biology, Brookhaven National Laboratory, Upton, New York 11973

Received November 7, 1997; Revised Manuscript Received January 26, 1998

ABSTRACT: The coronal structure of starlike block ionomer micelles has been probed directly by small-angle neutron scattering (SANS), using specific contrast labeling of different regions of the corona. Solutions of PS-*b*-**dPS**-*b*-PS-*b*-*PACs* starlike block ionomer micelles in toluene are studied; contrast is provided by perdeuterated polystyrene labels situated at different distances from the ionic core. For deuterated labels situated at 390 PS units from the core, the scattered intensity is found to scale as $I \sim q^{-1.7}$ at intermediate q, suggesting a semidilute environment for the labels and local swollen coil behavior. For labels 180 PS units from the core, steric perturbations are more extensive than those found under semidilute conditions, such that single chain scaling is not observed at any length scale; scattered intensity is found to scale as $I \sim q^{-1.3}$ at intermediate q. The stiffness of coronal chains next to the core is even greater, as indicated by $I \sim q^{-1.0}$ scaling for dPS labels attached directly to the ionic core; these probes exhibit rigid-rod behavior at length scales less than ca. 76 Å. In Kratky representations of the three samples, a maximum characteristic of polymer stars becomes more pronounced as the distance of the dPS labels from the core decreases, indicating greater contributions from interchain scattering. Increases in chain stiffness and interchain scattering suggest a significant increase in local segment densities with decreasing distance from the ionic core. Interparticle scattering as a function of polymer concentration is also investigated. The position of the Bragg peak scales with concentration as $c^{1/3}$, suggesting liquid ordering of the solution. Radii of gyration determined from Guinier analysis agree well with light scattering results, with the exception of micelles in which dPS probes are attached directly to the core. In this case, the neutrons "see" only the inner part of the spherical brush, and R_g from SANS data is less than R_g for the whole micelle.

1. Introduction

The structure of spherical polymer brushes has received a considerable amount of attention in recent years, spurred by industrial applications of such systems to colloid stabilization and surface modification. In several studies, model systems of star polymers[1−4] and starlike block copolymer micelles[5−10] have been employed in the investigation of spherical brushes, using small-angle X-ray scattering (SAXS) and small-angle neutron scattering (SANS). The latter experiment offers the advantage of deuterium labeling techniques, allowing for the determination of spatially specific information on brush structure. This strategy has been used to probe the structure of star polymers in which the inner cores and outer shells were selectively deuterated.[1,2] However, to our knowledge, this is the first study to employ deuterated labels for probing the coronal structure in block copolymer micelles.

Due to the high stability of block ionomer micelles, these materials provide an ideal system for the investigation of coronal structure. After micellization and complete neutralization of the ionic cores, the aggregates are essentially frozen structures, with no detectable equilibrium between micelles and single chains on a reasonable time scale.[11] It is therefore possible to study the spherical brushes under various conditions of solvent and polymer concentration without changes in the micelle aggregation numbers and core radii. Block ionomer micelles are thus very suitable models for polymer-protected colloidal particles, in which the ionic cores represent small spheres of ionic material, with a soluble stabilizing polymer (coronal chains) end-tethered to the particle surface.

In the present work, the coronal structure of starlike block ionomers is investigated, using deuterated labels at various distances from the ionic core. Using small-angle neutron scattering, three micelle samples with total coronal block lengths of ca. 800 units are studied; deuterated polystyrene (dPS) labels are situated at 0, 180, and 390 units from the core, such that the inner region of the polymer brush is probed in detail. Information on chain statistics is obtained from Kratky representations of the scattering profiles, and compared with predictions of the Daoud and Cotton model for starlike brushes.[12] All reverse micelles are studied under good solvent conditions; similar micelles under near-Θ conditions will be discussed in an upcoming publication. The effect of polymer concentration on the scattering profile in low and intermediate regions of the scattering vector is determined, providing insight into both spherical brush structure and interparticle correlations.

2. Experimental Section

2.1. Synthesis of PS-*b*-dPS-*b*-PS-*b*-PAA Block Copolymers. Block copolymers of the type PS-*b*-dPS-*b*-PS-*b*-PtBuA were prepared by the sequential anionic polymerization of

* Author to whom correspondence should be addressed.
[†] Present address: Department of Chemistry and Erindle College, University of Toronto, Toronto, Ontario, Canada M5S 1A1.
[‡] Department of Chemistry, McGill University.
[§] Department of Physics, Brookhaven National Laboratory.
[⊥] Department of Biology, Brookhaven National Laboratory.

S0024-9297(97)01646-X CCC: $15.00 © 1998 American Chemical Society
Published on Web 03/10/1998

styrene, perdeuterated styrene, and *tert*-butylacrylate in tetrahydrofuran (THF). The initiator was *sec*-butyllithium; lithium chloride (LiCl) and α-methylstyrene were added as capping agents for the "living" chains, to regulate anionic polymerization and prevent side reactions. Further details on sequential anionic polymerizations of this type are described in the literature.[11,13−15]

The degrees of polymerization of PS and dPS blocks, and the polydispersity indexes of the block copolymer samples (P.I.), were determined by size-exclusion chromatography (SEC). For all samples, P.I. values were between 1.08 and 1.13, indicating relatively low polydispersities for the polymer chains. The number of units in the poly(*tert*-butylacrylate) blocks were determined using quantitative FTIR (Perkin-Elmer 16 PC apparatus) of block copolymers dissolved in carbon tetrachloride. The poly(*tert*-butylacrylate) blocks were then hydrolyzed to the acid form, poly(acrylic acid) (PAA), by dissolving the polymers in toluene (5% polymer (w/w)) and refluxing for ca. 12 h in the presence of a *p*-toluenesulfonic acid catalyst. The hydrolyzed samples were precipitated into methanol and then dried under vacuum at 70 °C for ca. 24 h.

2.2. Preparation and Fractionation of Block Ionomer Micelles. Block copolymers in the acid form were dissolved in a 90/10 (v/v) mixture of benzene/methanol to obtain a solution of 2 wt % polymer. Micellization was induced by stoichiometric neutralization of the PAA blocks with a 0.25 M methanolic solution of cesium hydroxide monohydrate ($CsOH·H_2O$). The block ionomer micelles were then recovered by freeze-drying, followed by further drying of the samples under vacuum at 70 °C. Complete neutralization of the acid blocks to poly(cesium acrylate) (PACs) was confirmed by FTIR spectroscopy.

The reverse micelles in THF solutions were characterized by size-exclusion chromatography (SEC), using a Waters Model 510 liquid chromatograph equipped with a Varian RI-4 refractive index detector and the Millennium 2010 software package. Chromatograms revealed two populations at high and low elution volumes, attributed to single chains and micelles, respectively. The percentage of single chains with respect to the total weight of polymer was calculated from the relative areas under the two peaks. For the samples investigated, single chain fractions were between 15 and 28 wt %.

Single chain fractions in these block ionomers were attributed mainly to dPS-labeled polystyrene (i.e. no ionic block). Labeled, unmicellized chains will contribute to the coherent SANS scattering and may partially obscure the effects of coronal structure; it was therefore desirable to fractionate these materials, to obtain relatively pure micelle samples. Fractionation of the samples was accomplished by dissolving the samples to 2 wt % polymer in THF, followed by the addition of Milli-Q water (ca. 15% (w/w)); a white precipitate formed, and this was allowed to settle to the bottom of the container. Since micelles have a lower solubility in THF/water mixtures than single chains, the precipitate was assumed to contain mainly micellized material. The precipitate was isolated by vacuum filtration, dried under vacuum, and then characterized by SEC in THF solutions. SEC chromatograms revealed a significantly lower single chain fraction following fractionation. For some samples, the material was fractionated twice; final single chain fractions were ≤4 wt % in all cases.

The average lengths of the ionic blocks were significantly affected by the removal of the single chain fractions. For each sample, the average ionic block length was therefore recalculated, using FTIR data for the polymers in the ester form, and accounting for the weight percentage of labeled PS that was removed.

Three block ionomer samples were prepared for SANS experiments; these were designated samples I, II, and III, and had the following compositions: sample I, PS(240)-**dPS(190)**-PS(390)-*PACs(48)*; sample II, PS(370)-**dPS(250)**-PS(180)-*PACs(79)*; and sample III, PS(590)-**dPS(270)**-*PACs(60)*. Numbers in brackets designate degrees of polymerization for each block, with dPS labels indicated in bold characters and PACs blocks italicized for the sake of clarity. In later sections of this paper, polymer compositions will be shown using only degrees of polymerization for each block, e.g., sample I (240-**190**-390-*48*).

2.3. Static Light Scattering. Static light scattering experiments were performed on a Dawn-F multiangle laser photometer (Wyatt Technology) equipped with a He−Ne laser (632.8 nm). Data acquisition and Zimm plot processing was carried out using DawnF and Aurora (Wyatt) software, respectively. Stock solutions of samples I, II, and III were prepared by dissolving the white solids in toluene. These solutions were then filtered through membrane filters with a nominal pore size of 0.45 μm and transferred to a dust-free scintillation vial. Micelle solutions were diluted with filtered toluene, such that measurements were obtained at five different concentrations, in the range of 0.2−0.1 mg/mL.

2.4. Dynamic Light Scattering. Dynamic light scattering (DLS) experiments were performed on a Brookhaven Instruments photon correlation spectrometer equipped with a BI-9000AT digital correlator and Micro Green diode-pumped laser (532 nm) from Uniphase. All measurements were made in toluene at 22 °C over a range of concentrations 1.5−0.5 mg/mL. Stock solutions were filtered through membrane filters with a nominal pore size of 0.45 μm and transferred to dust-free vials. The angle of detection was 90° for all measurements.

Effective diffusion coefficients were determined from the first cumulant, which is the *z*-average relaxation rate, $\Gamma_z(s^{-1})$, of the autocorrelation function, $g_1(\tau)$. Values of the second cumulant, $\mu/\Gamma_z 2$, indicated relatively low polydispersities of relaxation rates for all three samples. Effective diffusion coefficients did not vary significantly in this range of concentrations, and were therefore assumed to be equivalent to D_0, the diffusion coefficient at infinite dilution. R_h values were calculated from D_0 using the Stokes−Einstein relation for diffusing spheres.

2.5. Small-Angle Neutron Scattering. SANS experiments were performed on a small-angle neutron scattering spectrometer (beamline NG7) in the cold neutron research facility at the National Institute of Standards and Technology (NIST). Sample to detector distances of 200 and 1350 cm were used, with a neutron wavelength of $\lambda = 6$ Å, to obtain scattering profiles in the regions $q = 0.012-0.30$ Å^{-1} and $q = 0.0020-0.030$ Å^{-1}, respectively. In the intermediate region ($q = 0.012-0.30$ Å^{-1}), samples I, II, and III were investigated in toluene solutions at polymer concentrations of 1, 3, and 5 wt %; the same solutions were investigated in the range of low q values ($q = 0.0020-0.030$ Å^{-1}), together with an additional dilute concentration (0.25 wt % polymer) for each sample.

Small-angle scattering data were collected using a 2D detector and normalized to a fixed number of incident neutrons corresponding to a monitor count of 10^8. The toluene background scattering was subtracted from the data, after which corrections for detector nonuniformity were performed through pixel-by-pixel division of the data by the measured scattering of water. A detector mask was applied to discard nonfunctional pixels and then the data were circularly averaged to obtain scattering profiles of the form I_{ave} vs q.

Scattering profiles were placed on an absolute scale by calculating $I_{abs}(q)$ from $I_{ave}(q)$, where $I_{abs}(q)$ is the absolute scattering cross section per unit volume of sample. For the remainder of this paper, the subscript "abs" is omitted in references to scattered intensity profiles, such that $I(q)$ represents the absolute scattering cross sections.

3. Results and Discussion

3.1. Static and Dynamic Light Scattering Results. Static light scattering data of samples I (240-**190**-390-*48*), II (370-**250**-180-*79*), and III (590-**270**-*60*) in toluene were used to construct Zimm plots, from which the radii of gyration, R_g, and molecular weights, M_w, of the micelles were determined. Since the weight fraction of single chains relative to total polymer was very low in all samples (≤4%), M_w values from Zimm

Table 1. Characteristics of Block Ionomer Micelles and Overlap Concentrations from Light Scattering Data

PS-*b*-**dPS**-*b*-PS-*b*-*PACs*	N_{PS}	Z	R_{core} (nm)	R_g (nm)	R_h (nm)	R_g/R_h	corona ext. (%)	c^*, fcc (wt %)	c^*, bcc (wt %)
sample I (240-**190**-390-*48*)	820	96	0.60	30	44	0.68	21	3.6	3.2
sample II (370-**250**-180-*79*)	800	110	0.70	33	46	0.72	22	3.8	3.4
sample III (590-**270**-*60*)	860	82	0.60	23	36	0.64	17	5.9	5.3

plot analysis were assumed to be equal to the molecular weights of reverse micelles; aggregation numbers, Z, for the three micelle samples were therefore calculated using values of M_w and the molecular weights of the component unimer chains. The radii of ionic cores, R_{core}, were calculated from aggregation numbers, assuming that the cores were spherical and free of solvent; in this calculation, the core density was equal to the measured bulk density of poly(cesium acrylate), 2 g/mL.[16] Considering strong ionic interactions in the core, and high surface tension at the core-solvent interface, exclusion of solvent from the ionic core is a reasonable assumption. Values of Z, R_{core}, and R_g for the three samples are listed in Table 1. Aggregation numbers range from 82 to 110, with core radii of 0.6 nm for samples I (240-**190**-390-*48*) and III (590-**270**-*60*) and 0.7 nm for sample II (370-**250**-180-*79*). The radii of gyration for samples I and II are very similar, 30 and 33 nm, respectively, while R_g for sample III, 23 nm, is somewhat lower.

To compare SANS profiles for deuterated labels at different positions within the micelle corona, all other micelle parameters should be held constant, especially those that influence the coronal structure. Values in Table 1 indicate that differences in aggregation numbers are not too significant, considering that the coronal brush height, H, is expected to scale only weakly with Z ($H \sim Z^{0.2}$ for starlike brushes);[12] however, a closer comparison of micelle structure in samples I, II, and III by light scattering techniques is worthwhile.

The hydrodynamic radius, R_h, provides useful information on the structure of micelles in solution. This quantity was determined from dynamic light scattering measurements in dilute solutions and therefore represents the overall radius of individual, noninteracting micelles. A combination of static and dynamic light scattering results allows the ratio R_g/R_h to be determined (Table 1), and this quantity yields useful information on the geometry of colloidal particles.[17] These values are found to be slightly less than the ratio for hard spheres ($R_g/R_h = 0.775$). Since anisotropic geometry, resulting from rod- or disklike structures, would result in ratios >0.775, these results seem to suggest spherical geometry of micelles for all three samples. It is not fully understood why R_g/R_h values (0.64−0.72) are somewhat less than those of hard spheres, though this may be related to long-range interactions in solution, resulting in slight increases in the apparent R_h, or to the existence of a free-draining term in the hydrodynamic behavior of the micelles.[17]

To determine the average extension of coronal chains in the micelle samples, the height of the spherical brush, H, was first calculated from

$$H = R_h - R_{core} \tag{1}$$

The percentage coronal extension (Table 1) was then obtained by comparison of the brush height with the fully extended contour length of PS chains,[18] as described in the expression

$$\% \text{ extension} = \frac{100H}{aN_{PS}} \tag{2}$$

where $a = 0.25$ nm, which is the length of one PS repeat unit; N_{PS} is the total number of PS and dPS units in a single coronal chain, which is between 800 and 860 units for all three samples. The percentage of extension in samples I (240-**190**-390-*48*) and II (370-**250**-180-*79*) were found to be very similar (21 and 22%) and these micelle populations were therefore assumed to have very similar coronal structures. The micelles in sample III (590-**270**-*60*), were found to have somewhat less extended coronae (17%), which can be attributed both to a lower aggregation number ($Z = 82$) and longer coronal chains ($N_{PS} = 860$). Fortuitously, the deuterated labels in sample III are located closest to the ionic core, where coronal chains are expected to be most severely stretched; the overall "less extended" structure of the micelle corona in this sample should therefore not obscure the effect of the label position.

Another parameter that can be determined from R_h is the micelle overlap concentration, c^*, which is simply the concentration at which the coronal regions of neighboring micelles begin to overlap. Calculations of c^* in toluene were made for both face-centered cubic (fcc) and body-centered cubic (bcc) packing of spheres[6,7,9] (where R_h = the radius of the spheres) (Table 1). Although interparticle correlations are considered in a later section of this paper, a detailed analysis of the structure factor is beyond the scope of the present work; therefore, the type of ordering at high polymer concentrations has not been confirmed, and values of c^* presented in Table 1 should be regarded as rough estimates of actual overlap concentrations. With these considerations, it was determined that micelle overlap in toluene begins at a polymer concentration of ca. 3 wt % for samples I (240-**190**-390-*48*) and II (370-**250**-180-*79*) and at ca. 5 wt % for sample III (590-**270**-*60*). In the discussion of SANS results, these results are compared with interparticle distances at different concentrations, as calculated from the Bragg peak of the structure factor.

3.2. Small-Angle Neutron Scattering Results. Corrected scattering profiles of I vs q for samples I (240-**190**-390-*48*), II (370-**250**-180-*79*), and III (590-**270**-*60*), in toluene can be attributed mainly to coherent scattering from the deuterated labels. This follows from relative scattering length densities of dPS labels (6.5×10^{-6} Å^{-2}), PS blocks (1.4×10^{-6} Å^{-2}), PACs cores (1.5×10^{-6} Å^{-2}), and toluene (0.9×10^{-6} Å^{-2}), which strongly suggest that the reverse micelles, with the exception of the deuterated labels, are contrast-matched with the surrounding solvent. Only the labels, therefore, are "seen" by the neutrons, although the labels themselves will "feel" the steric influence of both deuterated and undeuterated PS segments. It should be noted that the undeuterated material will contribute a considerable amount of incoherent scattering to the raw data, although this component is removed in the data reduction process, by subtraction of the solvent background.

The coherent scattered intensity consists of both interparticle and intraparticle contributions, known as the structure factor, $S(q)$, and form factor, $P(q)$, respectively:

$$I(q) \sim S(q)P(q) \tag{3}$$

The interparticle structure factor is the Fourier transform of the pair correlation function, $g(r)$

$$S(q) = 1 + \frac{4\pi}{\rho}\int r[g(r) - 1]\sin(qr)\,dr \tag{4}$$

where ρ is the particle number density of micelles. At high values of the scattering vector, the structure factor asymptotically approaches unity, and the form factor becomes the dominant contribution to coherent scattering. As well, the structure factor becomes insignificant at extremely low concentrations, where correlations between particles are negligible. At sufficient degrees of dilution, therefore, it is possible to relate the scattered intensity at low q values to intraparticle scattering; this is known as the Guinier region of the form factor, and yields the radius of gyration of individual particles.

The following section is divided into three parts. In section 3.2.1, scattered intensity profiles at intermediate q values are discussed, and the contribution of interparticle scattering in this region is considered. Analysis of $I(q)$ yields information on the structure and stiffness of deuterated labels within the micelle corona, and comparison of the samples allows these parameters to be determined as a function of distance from the ionic core. In section 3.2.2, the intensity $I(q)$ is considered at low values of the scattering vector, where the effect of interparticle scattering becomes significant. The structure factor is discussed as a function of polymer concentration. Finally, in section 3.2.3, the form factors at low q values are recovered, by sufficient dilution of the samples; radii of gyration are calculated from the Guinier region of the scattering profiles and compared with values obtained from light scattering data.

3.2.1. Coronal Structure of Block Ionomer Micelles. In the intermediate region of the scattering vector, corrected profiles $I(q)$ obtained at 1, 3, and 5 wt.% polymer were normalized with concentration; most plots of I/c vs q for identical samples at different concentrations show excellent superposition (Figure 1). This suggests that the scattered intensity in this region is dominated by the form factor, $P(q)$, and is therefore not influenced by interparticle concentration effects. The one exception appears to be sample I (240-**190**-390-*48*) at the highest polymer concentration (5 wt %), where negative deviations in the scattering profile are observed at vectors below $q \sim 0.05$ Å^{-1}, possibly due to structure factor contributions.

For a polymer concentration of 3%, the scattering profiles for samples I (240-**190**-390-*48*), II (370-**250**-180-*79*), and III (590-**270**-*60*) were compared in the form of Kratky representations, $Iq^{5/3}$ vs q (Figure 2). For polymer chains in Θ-solvents, Kratky plots are typically in the form Iq^2 vs q; however, in the present case of a good solvent, the exponent, 5/3, was chosen based on the expected intensity scaling for swollen chains in the intermediate region of the scattering vector ($I \sim q^{-5/3}$). It should be stressed that the most significant difference between samples I, II, and III is the position of the deuterated label, which is located at 390, 180, and 0 PS units, respectively, from the ionic core. For sample I

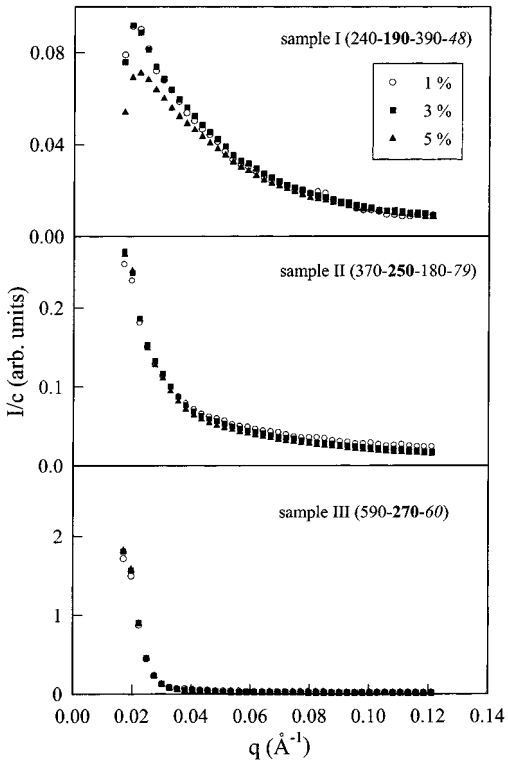

Figure 1. Scattered intensity normalized with concentration, $I(q)/c$ (1, 3, and 5 wt % polymer), vs scattering vector in the intermediate region.

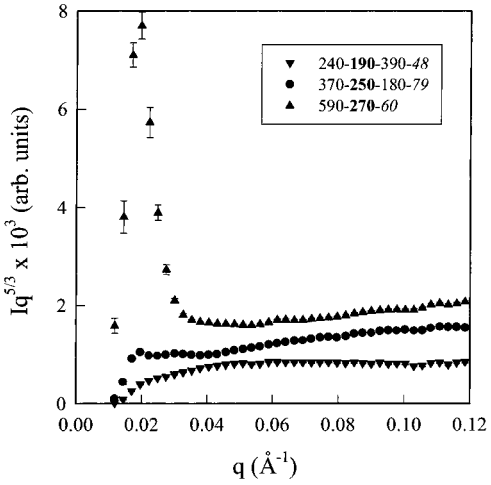

Figure 2. Kratky plots for samples I (240-**190**-390-*48*), II (370-**250**-180-*79*), and III (590-**270**-*60*), at a concentration of 3 wt %. Only sample I (▼) approaches the $q^{-5/3}$ scattering of swollen coils.

(240-**190**-390-*48*), the Kratky plot approaches a horizontal asymptote, indicating $q^{-5/3}$ scaling above $q^* \sim 0.05$ Å^{-1}. This is in agreement with the Daoud and Cotton model of starlike brushes, in which polymer chains are represented by a string of "blobs" of radially increasing size; within these blobs, scattered intensity scales as $I \sim q^{-5/3}$, in the manner of isolated swollen coils.[12] However, from the Kratky plots of samples II (370-**250**-180-*79*) and III (590-**270**-*60*), it can be seen that scattering from the deuterated labels does not approach $q^{-5/3}$ scaling, as evinced by a steady increase of $Iq^{5/3}$ with increasing q.

Another distinct feature in Kratky plots of samples II (370-**250**-180-*79*) and III (590-**270**-*60*) is a maximum at $q \sim 0.02$ Å^{-1}, which is significantly more pronounced

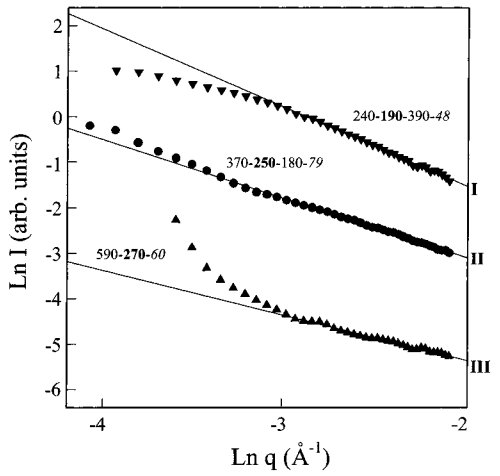

Figure 3. SANS profiles on a natural log scale for samples I (240-**190**-390-*48*), II (370-**250**-180-*79*), and III (590-**270**-*60*), at a concentration of 3 wt %. Solid lines indicate linear regression in the region ln $q > -3$ ($q > 0.05$ Å^{-1}); the slopes of the lines yield characteristic exponents for the scaling relation $I \sim q^{-\alpha}$.

Table 2. $I(q)$ Scaling Exponents ($I \sim q^{-a}$) at Intermediate Scattering Vectors, for Deuterated Labels in Block Ionomer Micelles

*PS-b-***dPS**-*b*-PS-*b-PACs*	poly. conc. (wt %)	α, $q > 0.05$ Å^{-1}
sample I (240-**190**-390-*48*)	1	1.8
sample II (370-**250**-180-*79*)	1	1.0
sample III (590-**270**-*60*)	1	0.7
sample I (240-**190**-390-*48*)	3	1.7
sample II (370-**250**-180-*79*)	3	1.3
sample III (590-**270**-*60*)	3	1.0
sample I (240-**190**-390-*48*)	5	1.7
sample II (370-**250**-180-*79*)	5	1.4
sample III (590-**270**-*60*)	5	1.1

in the latter sample. This peak is an expected feature for fully contrasted stars, and in Benoit's model of Gaussian stars, it occurs at $q \sim 1/R_g$.[19] The scattered intensity will increasingly resemble that of a polymer star as contributions from interchain scattering become more prominent; this will occur as the local segment densities of the contrasted labels increase. Thus the clear growth of the Kratky maximum suggests higher local segment densities for dPS probes situated closer to the core. In star polymer systems, Kratky maxima were also found to be more pronounced when the contrast of the inner brush was increased.[2] Gast and co-workers observed maxima in Kratky plots for symmetrical PS-*b*-PEO micelles in cyclohexane/water; no contrast labeling was used in that study, although average densities of coronal regions were high enough to show evidence of significant scattering between chains.[5]

A quantitative comparison of I vs q in the intermediate region of the scattering vector was obtained by plotting SANS profiles on a natural log scale. Such plots for micelles at 3 wt % polymer are shown in Figure 3. For all three samples, the profiles exhibit linear behavior above ln $q = -3$ ($q > 0.05$ Å^{-1}); slopes obtained from least squares regression of the linear regions yield scaling exponents for $I \sim q^{-\alpha}$, where α is termed the characteristic exponent, and these are listed in Table 2. As described earlier, a swollen coil is expected to show scattered intensity scaling as $I \sim q^{-5/3}$ ($\alpha = 5/3$ or 1.7) in the intermediate region of q; this is also true of semidilute solutions in good solvents, which show local swollen coil behavior at length scales shorter than the blob size. In general, stiffer chains will show lower values of the characteristic exponent, with $\alpha = 1$ indicating rodlike scaling at certain length scales.

At 3 wt %, a value of $\alpha = 1.7$ was determined for sample I (240-**190**-390-*48*), confirming the results of Kratky analysis and suggesting a semidilute environment for dPS labels 390 units from the core. At the same polymer concentration, scattering from dPS labels 180 units from the core (sample II) gave $\alpha = 1.3$, indicating $I \sim q^{-1.3}$ scaling for $q > 0.05$ Å^{-1}; thus the stiffness of chains is markedly higher in this region of the corona, such that the labels no longer exhibit single chain behavior at intermediate q. The environment of the labels is no longer semidilute, and steric perturbations to chain conformations are more severe. This trend is further demonstrated by scattered intensity for sample III (590-**270**-*60*) at the same concentration (3%), which shows rodlike scaling, $I \sim q^{-1.0}$, for scattering vectors greater than 0.05 Å^{-1}. From the minimum scattering vector for $q^{-1.0}$ scaling,[20] $q = 0.05$ Å^{-1}, it is determined that the dPS labels next to the core can be described in terms of statistical units of ca. 75 Å in length; this value can be compared with the fully extended contour length of the dPS labels (270 units), which is 675 Å. Each label contains only nine statistical units and will therefore behave in a "wormlike", rather than a statistical, manner.

The observed increase in the stiffness of dPS labels with decreasing distance from the core can be attributed to higher local segment densities closer to the center of the polymer brush. This supports the results of Kratky analysis and suggests a segment density profile which decreases with radial distance from the center, as predicted by Daoud and Cotton in their model of starlike polymer brushes. However, by labeling different parts of the corona in block copolymer micelles, it has also been shown that the "blob" concept of that model can only be applied at distances sufficiently removed from the core, where coronal chains exist in a semidilute environment. Close to the core of starlike micelles, high segment densities result in large steric perturbations to swollen coil behavior, such that $q^{-5/3}$ scaling of scattered intensity is not observed on any length scale. A breakdown of the blob model near the core of starlike block copolymer micelles has been predicted by Gast et al.;[5] to our knowledge, this work provides the first direct support of that prediction.

Values of characteristic exponents for the relation $I \sim q^{-\alpha}$, where $q > 0.05$ Å^{-1}, are listed in Table 2 for different polymer concentrations. For all samples, it is found that the values obtained for 5% and 3% solutions are nearly identical, indicating an absense of interparticle effects on the statistics of the deuterated labels. It should be noted that micelle−micelle interactions may affect the overall structure of the corona at the higher polymer concentration (5%), even though this effect is not observed in the deuterated labels. This is possible since the dPS labels may be screened from overlap effects, due to relatively high local segment densities close to the core.

We further note that samples II (370-**250**-180-*79*) and III (590-**270**-*60*) show somewhat depressed characteristic exponents ($\alpha = 1.0$ and 0.7, respectively) at polymer concentrations of 1%. These effects are believed to be artifacts resulting from extremely low scattering intensities, in particular at high q values, from dPS probes in the 1% solutions. In the case of sample III, the measured exponent, $\alpha = 0.7$, is not physically meaning-

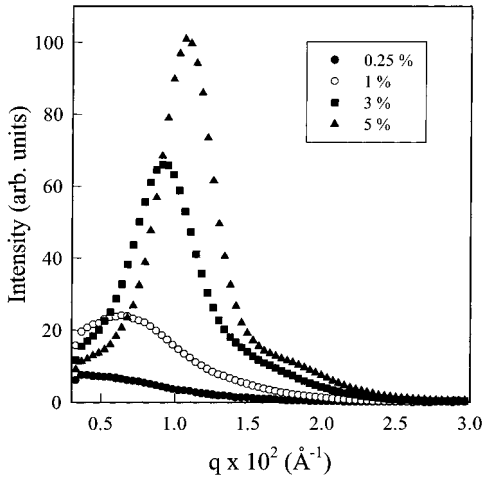

Figure 4. SANS profiles in low-q region, for sample III (590-**270**-*60*) at different polymer concentrations. The Bragg peak (observed for 1, 3, and 5 wt % solutions) is found to shift to higher q as the concentration is increased.

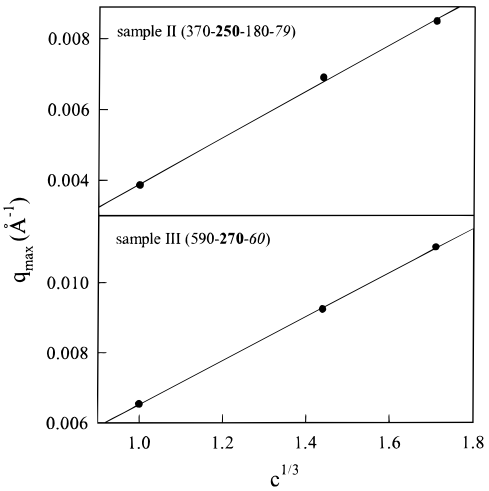

Figure 5. Plots of the Bragg peak position, q_{max}, vs $c^{1/3}$ for samples I and II. The linear relation indicates liquid ordering in these solutions.

Table 3. Comparison of Interparticle Distances and Micelle Hydrodynamic Diameters

PS-*b*-**dPS**-*b*-PS-*b*-*PACs*	polym concn (wt %)	$2R_h$ (nm)	$q_{max} \times 10^2$ (Å^{-1})	d_{Bragg} (nm)
sample I (240-**190**-390-*48*)	1	88	0.42	149
sample I (240-**190**-390-*48*)	3	88	0.77	82
sample I (240-**190**-390-*48*)	5	88		
sample II (370-**250**-180-*79*)	1	92	0.39	163
sample II (370-**250**-180-*79*)	3	92	0.69	91
sample II (370-**250**-180-*79*)	5	92	0.85	74
sample III (590-**270**-*60*)	1	72	0.65	96
sample III (590-**270**-*60*)	3	72	0.92	68
sample III (590-**270**-*60*)	5	72	1.10	57

ful, as the smallest possible exponent is $\alpha = 1.0$ for rodlike scaling.

3.2.2. Interparticle Scattering and Solution Structure. In the range of low q values ($q = 0.0020-0.030$ Å^{-1}), scattered intensity from dPS probes revealed clear interparticle correlations for most polymer concentrations. Plots of I vs q in this region are shown for sample III (590-**270**-*60*) at polymer concentrations of 0.25, 1, 3, and 5 wt % (Figure 4). Except for the lowest concentration, a maximum is observed in all SANS profiles; this is the first-order structure peak, or Bragg peak, and is related to the average distance between particles, d_{Bragg}, by

$$d_{Bragg} = 2\pi/q_{max} \quad (5)$$

where q_{max} is the position of the first structure factor maximum. From Bragg peak positions, d_{Bragg} was calculated for the three samples at polymer concentrations of 1, 3, and 5 wt % (Table 3); due to overlap with the form factor, the Bragg maximum for sample I at 5 wt % was not clearly defined and is therefore not reported in Table 3.

In order for micelle overlap to occur, the average distance between particles, d_{Bragg}, must be equal to or less than twice the particle radius. Hydrodynamic diameters from dynamic light scattering results, $2R_h$, are therefore listed alongside d_{Bragg} values (Table 3). The hydrodynamic radii, R_h, are defined for dilute conditions, as they describe the overall size of isolated micelles in solution; as indicated in Table 3, these values do not vary with polymer concentration. Comparison of $2R_h$ and d_{Bragg} indicates that the condition of micelle overlap, $2R_h = d_{Bragg}$, is fulfilled for all three samples at a polymer concentration of ca. 3%. For samples I (240-**190**-390-*48*) and II (370-**250**-180-*79*), this finding agrees well with c^* values in Table 1, which were calculated using the assumption of a cubic lattice for solution ordering. Using the same assumption, c^* for sample III (590-**270**-*60*) was determined to be ca. 5%, which is higher than the value of ca. 3% from Bragg spacings. A possible reason for this discrepancy is the lower percentage of extension for coronal chains in sample III (Table 1), which may allow the particles to pack into a somewhat less ordered lattice type.

For samples II and III, the position of the Bragg maximum, q_{max}, was plotted vs $c^{1/3}$, where c is the weight percent polymer concentration; a linear relation was obtained in both cases (Figure 5). This supports the existence of liquid order in the system, for which q_{max} is expected to scale as $c^{1/3}$; sample I was not included in this analysis, since only two data points were available.

A more detailed description of solution structure would require fitting of the form factor, $P(q)$, in the region of low q, such that $S(q)$ could be mathematically extracted from the corrected scattering profile $I(q)$, according to eq 3. In this case, higher-order structure peaks may be detected at high concentrations, which, in principle, would allow determination of the micelle packing lattice. In another study,[21] SAXS profiles of PS-*b*-PACs reverse micelles were obtained at various solution concentrations and in the bulk; isolated structure factors revealed up to three peaks related to interparticle correlations. The systems were found to exhibit liquid order, although the exact structure of the solutions could not be solved.

3.2.3. Guinier Analysis. Guinier plots were also constructed from SANS profiles in the region of low q, using data obtained at a polymer concentration of 0.25 wt %. At this degree of dilution, $I(q)$ did not show evidence of interparticle scattering for any of the samples; in Figure 4, the Bragg maximum has completely disappeared at 0.25%, suggesting that the form factor, $P(q)$, has been recovered at low q. When interparticle effects are negligible, the particle radius of gyration can be determined from the scattered intensity profile at small scattering vectors, according to the

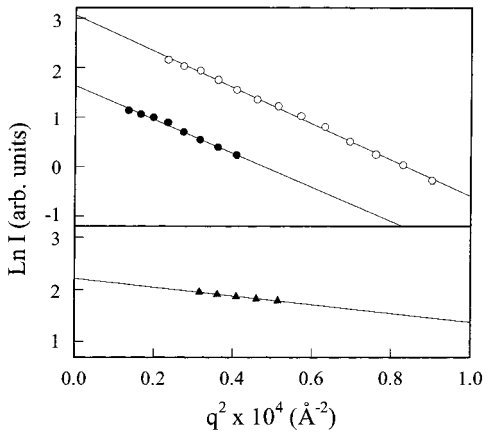

Figure 6. Guinier plots, ln I vs q^2, for sample I (○), II (●), and III (▲) at a polymer concentration of 0.25 wt %.

Guinier approximation:

$$I(q) = I(0) \exp[-q^2 R_g^2/3] \quad (6)$$

Radii of gyration for the three samples were thus obtained from slopes of ln $I(q)$ vs q^2 in selected linear regions at low q. These plots are shown in Figure 6 for samples I (240-**190**-390-*48*), II (370-**250**-180-*79*), and III (590-**270**-*60*), and yield R_g values of 32, 33, and 16 nm, respectively. The values for samples I and II agree well with those obtained from static light scattering measurements 30 and 33 nm (Table 1), which suggests that neutron scattering in the Guinier regime reflects the size of the overall micelle, rather than individual deuterated labels; this follows from the mobility of the polymer chains, which should allow the labels to "explore" all parts of the micelle corona, even though their average local densities are governed by their most probable position within the brush. In sample III, however, the dPS labels are linked directly to the ionic core, such that their mobility within the corona is restricted to the inner polymer brush. The radius of gyration from Guinier analysis of the SANS profile (16 nm) is therefore somewhat smaller than R_g of the whole micelle (23 nm), as determined by static light scattering.

Since the ionic core is very small (R_{core} = 0.60 nm) compared with the size of the brush, the contrast situation in sample III (590-**270**-*60*) allows the neutrons to "see" what resembles a dense star polymer, with 82 arms of 270 dPS units radiating out from a single point. From the radius of gyration of this star, R_g = 16 nm, the radius of gyration of each individual arm[22] was calculated using the expression

$$\frac{R_{g,star}}{R_{g,arm}} = \left[\frac{(3Z-2)}{Z}\right]^{1/2} \quad (7)$$

where the value inside the square brackets equals 2.98 when Z = 82. The radius of gyration of the deuterated arms in sample III was thus determined to be 9.3 nm. As expected, this value lies between the radius of gyration of a "free" dPS label of equivalent length in toluene (5 nm), and that of the fully extended label (19 nm). It is also useful to compare the radius of gyration of the star from Guinier analysis, R_g = 16 nm, with the value determined from the Kratky peak in Figure 2, which should occur at $1/R_g$ for Gaussian stars.[19] The latter method yields R_g = 5 nm, more than three times smaller than the Guinier result. This suggests that the Gaussian model does not apply to the tightly packed star in sample III (590-**270**-*60*).

4. Conclusions

Small-angle neutron scattering (SANS) experiments were used to study solutions of PS-*b*-**dPS**-*b*-PS-*b*-*PACs* starlike block ionomer micelles in toluene, in which contrast was provided by deuterated labels situated at different distances from the ionic core. Characteristic exponents for the scaling relation $I \sim q^{-\alpha}$ were determined from corrected scattering profiles at intermediate scattering vectors. For deuterated labels situated at 390 PS units from the core, the scattered intensity scaled as $I \sim q^{-1.7}$ at intermediate q, suggesting a semidilute environment for the labels and local swollen coil behavior. When the probes were 180 PS units from the core, however, they did not show single chain scaling at any length scale, and the relation $I \sim q^{-1.3}$ was found at intermediate q. The stiffness of dPS probes directly attached to the core was even greater; in this case, $I \sim q^{-1.0}$ scaling indicated wormlike chains with statistical units of ca. 75 Å. In Kratky representations of the three samples, a maximum characteristic of polymer stars was found to be more pronounced for dPS labels located closer to the core, indicating greater contributions from interchain scattering. The observed increases in chain stiffness and interchain scattering suggest a significant increase in local segment densities with decreasing distance from the ionic core, in agreement with the Daoud and Cotton model for star polymers. However, in the present case of starlike block ionomer micelles, it is found that the use of "blobs" of local single chain behavior to describe the polymer brushes is applicable only at distances sufficiently removed from the core.

In the region of low q, interparticle scattering was investigated as a function of polymer concentration. From the position of the Bragg maximum, the average distance between particles was calculated, and the concentration at which $2R_h = d_{Bragg}$ was estimated. For samples I (240-**190**-390-*48*) and II (370-**250**-180-*79*), overlap concentrations, c^*, determined in this manner agreed with values calculated for body and face-centered lattices of micelle packing. The position of the Bragg peak was found to scale with concentration as $c^{1/3}$, suggesting liquid ordering of the solution.

Radii of gyration determined from Guinier analysis agreed well with light scattering results for samples I (240-**190**-390-*48*) and II (370-**250**-180-*79*). In sample III (590-**270**-*60*), however, in which the labels were attached directly to the core, R_g from SANS (16 nm) was smaller than the value determined for micelles by static light scattering (23 nm). In this case, the neutrons "see" only the inner part of the spherical brush, which resembles a densely packed star polymer. R_g for a single dPS arm of the star was determined to be 9.3 nm, which lies between values for the equivalent free swollen coil (5 nm) and the fully extended chain (19 nm).

Acknowledgment. This work was supported by the Natural Sciences and Engineering Research Council of Canada (NSERC). The authors would like to acknowledge Drs. John Barker and Charlie Glinka for their assistance with the small angle neutron spectrometer. M.M. is grateful for scholarship funding provided by NSERC and Le Fonds pour la Formation de Chercheurs et l'Aide à la Recherche (FCAR, Quebec).

References and Notes

(1) Lantman, C. W.; MacKnight, W. J.; Rennie, A. R.; Tassin, J. F.; Monnerie, L. Fetters, L. J. *Macromolecules* **1990**, *23*, 836.
(2) Richter, D.; Farago, B.; Fetters, L. J.; Huang, J. S.; Ewen, B. *Macromolecules* **1990**, *23*, 1845.
(3) Dozier, W. D.; Huang, J. S.; Fetters, L. J. *Macromolecules* **1991**, *24*, 2810.
(4) Willner, L.; Jucknischke; Richter, D.; Roovers, J.; Zhou, L.-L.; Toporowski, P. M.; Fetters, L. J.; Huang, J. S.; Lin M. Y.; Hadjichristidis, N. *Macromolecules* **1994**, *27*, 3821.
(5) Cogan, K. A.; Gast, A. P.; Capel, M. *Macromolecules* **1991**, *24*, 6512.
(6) McConnell, G. A.; Gast, A. P.; Huang, J. S.; Smith, S. D. *Phys. Rev. Lett.* **1993**, *71*, 2102.
(7) McConnell, G. A.; Lin, E. K.; Gast, A. P.; Huang, J. S.; Lin, M. Y.; Smith, S. D. *Faraday Discuss.* **1994**, *98*, 121.
(8) Förster, S.; Wenz, E.; Lindner, P. *Phys. Rev. Lett.* **1996**, *77*, 95.
(9) Gast, A. P. *Langmuir* **1996**, *12*, 4060.
(10) McConnell, G. A.; Gast, A. P. *Macromolecules* **1997**, *30*, 435.
(11) Desjardins, A.; Eisenberg, A. *Macromolecules* **1991**, *24*, 5779.
(12) Daoud, M.; Cotton, J. P. *J. Phys.* **1982**, *43*, 531.
(13) Long, T. E.; Allen, R. D.; McGrath, J. E. In *Chemical Reactions On Polymers*; Benham, J. L., Kinstel, J. F., Eds.; ACS Symposium Series 364; American Chemical Society: Washington, DC, 1988; Chapter 19.
(14) Gauthier, S.; Duschesne, D.; Eisenberg, A. *Macromolecules* **1987**, *20*, 753.
(15) Zhong, X. F.; Varshney, S. K.; Eisenberg, A. *Macromolecules* **1992**, *25*, 7160.
(16) Nguyen, D.; Williams, C. E.; Eisenberg, A. *Macromolecules* **1994**, *27*, 5090.
(17) Burchard, W. *Adv. Polym. Sci.* **1983**, *48*, 1.
(18) Zhang, L.; Barlow, R. J.; Eisenberg, A. *Macromolecules* **1995**, *28*, 6055.
(19) Benoit, H. *J. Polym. Sci.* **1953**, *11*, 507.
(20) Kratky, O. *Pure Appl. Chem.* **1966**, *12*, 483.
(21) Nguyen, D.; Varshney, S. K.; Williams, C. E.; Eisenberg, A. *Macromolecules* **1994**, *27*, 5086.
(22) Burchard, W.; Kajiwara, K.; Nerger, D.; Stockmayer, W. H. *Macromolecules* **1984**, *17*, 222.

MA971646N